Chapter 2

Spontaneous chiral symmetry breaking and novel growth patterns exhibited by smectic-C domains of a binary mixture

2.1 Introduction

In this chapter, we describe the observation of spontaneous chiral symmetry breaking in three-dimensional domains of a smectic-C liquid crystal coexisting with the nematic phase. This new *'chiral'* structure was observed in a binary mixture made up of *achiral* molecules. The smectic-C domains exhibited a helical structure with a surface disclination line which coiled around the domain surface. Both left-handed and right-handed domains formed with equal probability. The detailed structure of these domains was established using microscopic observations, xray diffraction studies, response to external electric fields, etc. We have also demonstrated that the application of a chiral bias field in the form of a twist distortion in the director-field of the surrounding nematic medium produces chiral discrimination. The highly anisotropic growth of these domains was also studied in some detail. **A** theoretical analysis of the helical structure of these domains and of the unusual growth pattern are presented in the next chapter.

Before going into the experimental details, we first give a brief description of the observations of chiral symmetry breaking and growth patterns in a few other systems.

2.1.1 Spontaneous chiral symmetry breaking

The phenomenon of spontaneous chiral symmetry breaking is well known in crystals and has been studied since the time of Louis Pasteur [13]. More recently there have been several reports on this phenomenon occurring in a wide range of materials like sodium chlorate crystals [14], drops of nematic [15] and smectic-C [16] liquid crystals, thin films of smectic-C liquid crystals [17] and Langmuir monolayers with tilt order [18]. In the case of sodium chlorate, Kondepudi et. al. [14] demonstrated for the first time that a chiral bias produced by the constant stirring of the solution during crystal formation produced an asymmetric state having unequal number of right and left handed crystallites. The mechanism responsible for the chiral discrimination in this case is not well understood [19]. Drops of nematic liquid crystals coexisting with the isotropic phase (or suspended in an immiscible liquid) usually show either a 'hedge hog' or a 'bipolar' structure depending on whether the surface anchoring is normal or tangential, respectively. Press and Arrot [15] have shown that in nematic drops floating on water, apart from the perfect hedge hog patterns, structures with either a right handed or a left handed twist can also occur. They have attributed this twist deformation to a splay cancellation mechanism. Kurik and Lavrentovich [20] have reported twisted bipolar structures in drops of a nematic liquid crystal suspended in glycerine. Similar structures have also been observed in drops of smectic-C liquid crystals floating on the isotropic melt in the presence of a strong temperature gradient [16]. Recently, Pang and Clark [17] have reported the observation of periodic twist-bend instability, which results in chiral domains, in freely suspended smectic-C films. According to them, this instability arises due to a polar ordering of the molecules at the smectic-air interface and packing considerations of molecules with a bulky perfluoro chain on one side and a perhydro chain on the other. Apart from this, there have been observations of spontaneous chiral symmetry breaking in other quasi-two-dimensional systems like

Langmuir monolayers [18] and hexatic liquid crystal films [21] with tilt order. Many of these $2D$ structures are explained by a Landau theory developed by Selinger *et. al.* [22].

The chiral symmetry breaking we have studied occurs in *three-dimensional* domains of a SmC liquid crystal which results in a *periodic* structure with a well defined handedness and pitch. This is in contrast with earlier examples in which periodic structures were seen only in two-dimensional systems and the periodicity was due to alternating 'chirality'. Also, as will be discussed in the next chapter, the mechanism responsible for the formation of the periodic structure is different from those mentioned above.

2.1.2 Growth patterns in smectics

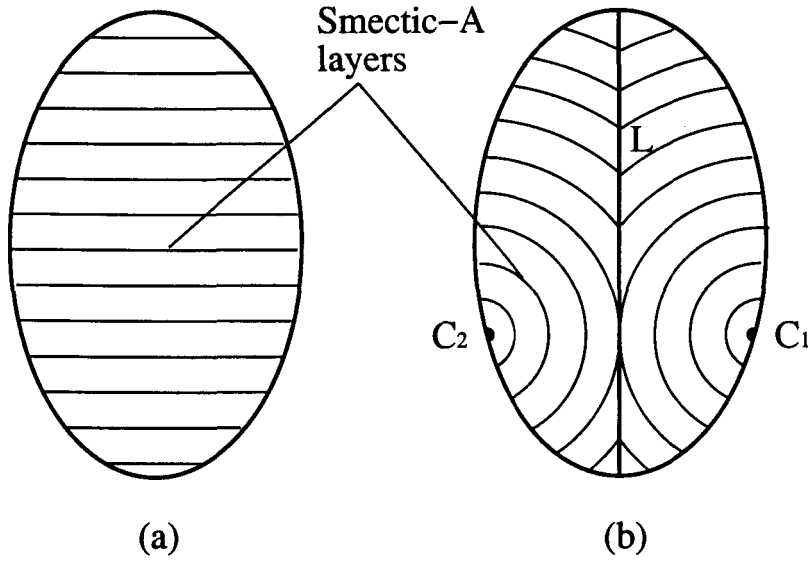

Figure 2.1: (a) A smectic-A domain with undistorted layers. Although there is no elastic energy cost for creating such a structure, the interfacial energy cost can be large due to the non-zero angles the director makes with the interface. (b) The smectic layering in a focal-conic domain. The structure is cylindrically symmetric about the disclination line, L. The points C_1 and C_2 represent the intersection of the surface disclination loop with the plane of the figure. Note that in this structure the director is more or less parallel to the interface. The focal-conic structure is preferred over the uniform one beyond a critical domain size when the surface energy dominate over the bulk elastic energy.

Apart from exhibiting chiral symmetry breaking, the growth patterns shown by these domains is also very unusual. Smectic liquid crystals have highly anisotropic surface tension. For example, for a smectic-A–isotropic or smectic-A–nematic interface, the surface tension for a surface oriented parallel to the smectic layers, $\gamma_{\|}$, is usually several times larger than that for a surface oriented perpendicular to the plane of the layers, $\gamma_{\perp}$. In the case of smectic-C there are three principal values of surface tension since the medium is biaxial. Also, unlike crystals, the smectic layers can be deformed without altering the layer periodicity. The energy cost for this deformation is several orders of magnitude lower compared to that for changing the layer spacing. In the case of smectic-C, there is an additional degree of freedom, namely, the orientation of the c-vector. As a result of these properties smectic liquid crystals can exhibit a variety of growth patterns [23, 24, 25]. The most commonly seen are the so called 'biitonnets' which form when smectic domains are nucleated from the nematic or the isotropic phase [26]. Biitonnets are 'equilibrium shapes' and the domain can be viewed as part of a 'focal-conic' (also called Dupin cyclide) structure (Fig. 2.1). Such a structure is favoured above a critical domain size as it lowers the interfacial energy by exposing only the surface that has the least interfacial tension. In the case of smectic-C, the Bâtonnet structure is more complicated due to deformations in the c-director field [23]. As these domains grow they take more and more complicated shapes [27] and finally merge and form the focal-conic texture in the case of smectic-A and the 'broken' focal-conic texture in the case of smectic-C liquid crystals [26].

The structure and shape of the new type of domains we have observed are very different from those of biitonnets. The domains are highly elongated and each of them has a helical band wrapped around it. On lowering the temperature, they grow rapidly along their long axes. At even lower temperatures they merge and form large uniform strips separated by sharp walls.

In this chapter we also describe some unusual features in the nucleation and growth of these domains. The theoretical analysis is presented in the next chapter.

2.2 Experimental studies

The experiments were performed on a binary mixture of the achiral compounds, namely, p-heptyloxy benzylidene p-heptylaniline (70.7) and 2-cyano-4-heptylphenyl-4'-pentyl-4-biphenyl carboxylate ($7CN5$) obtained from Merck. The molecular structures of these two compounds are shown in Fig. 2.2.

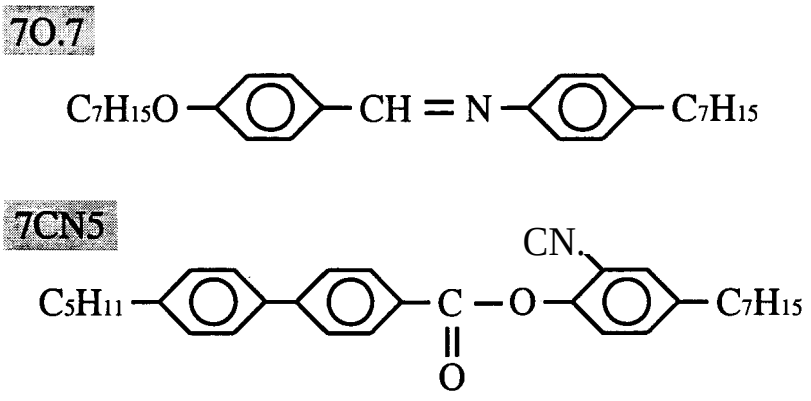

Figure 2.2: Molecular structures of the compounds used in the experiments.

The first component, 70.7, shows a variety of phases, including the SmC phase in the following sequence as a function of temperature (in ^oC): Cr – 33 – SmG – 55 – SmB – 69 – SmC – 71.7– SmA – 83.3 – N – 83.8 – I [28], where SmB is a smectic phase with hexatic order [1, 2] within the layers. SmG and K denote three dimensional crystals. The second component, $7CN5$, has the following phase sequence (temperatures are in ^oC): Cr – 45.5 – N – 102.0 – **I.** The nematic phase of $7CN5$ has a strong **skew-cybotactic** (SmC-like) short range order [1] and supercools down to room temperature [29]. Mixtures of these two compounds, in a certain composition range, show a first order N-SmC transition. The detailed phase diagram for the mixtures is shown in Fig. 2.3. The transition temperatures were measured using a Mettler FP80 hot-stage while cooling at a rate of $0.1^oC/min$ and

correspond to the appearance of the first domain of the lower temperature phase. The coexistence region, which was very wide for the N-SmC transition in particular, is not indicated in the diagram. Also transitions to hexatic SmB, etc are not shown as they are not relevant to the present problem.

The phase diagram shows that the addition of $7CN5$ reduces the SmA temperature range and also lowers the SmA-SmC transition temperature. Above $15wt\%$ of $7CN5$ there is a direct transition from the nematic to the SmC till around $38wt\%$ of $7CN5$ beyond which the nematic phase extends down to room temperature. Also, note that there is a minimum in the isotropic to nematic transition temperature at around $20wt\%$ of $7CN5$. This is probably due to the difference in the type of short range order exhibited by the two pure compounds. The mixtures showed a large N-SmC coexistence range which increased with increase in the concentration of $7CN5$.

Most of the experiments reported in the following sections, unless otherwise specified, were conducted on a mixture with $31.7wt\%$ of $7CN5$. This mixture showed the following phases on cooling (temperatures are in ^oC): $I - 80.8 - N - 36.1 - SmC$. The N-SmC coexistence range for this composition was found to be more than 5^oC. Also, on cooling from the isotropic phase the nematic always formed near the surface of the glass plates. But, on cooling below the N-SmC transition point, the smectic domains always nucleated near the mid-plane of the cell. This indicates that the $7CN5$ wets the treated glass plates better than 70.7 as its concentration was higher near the surfaces of the cell. From the phase diagram it is clear that a higher concentration of $7CN5$ will increase the I-N transition temperature and lower the N-SmC transition temperature for mixtures with more than about $20wt\%$ of $7CN5$.

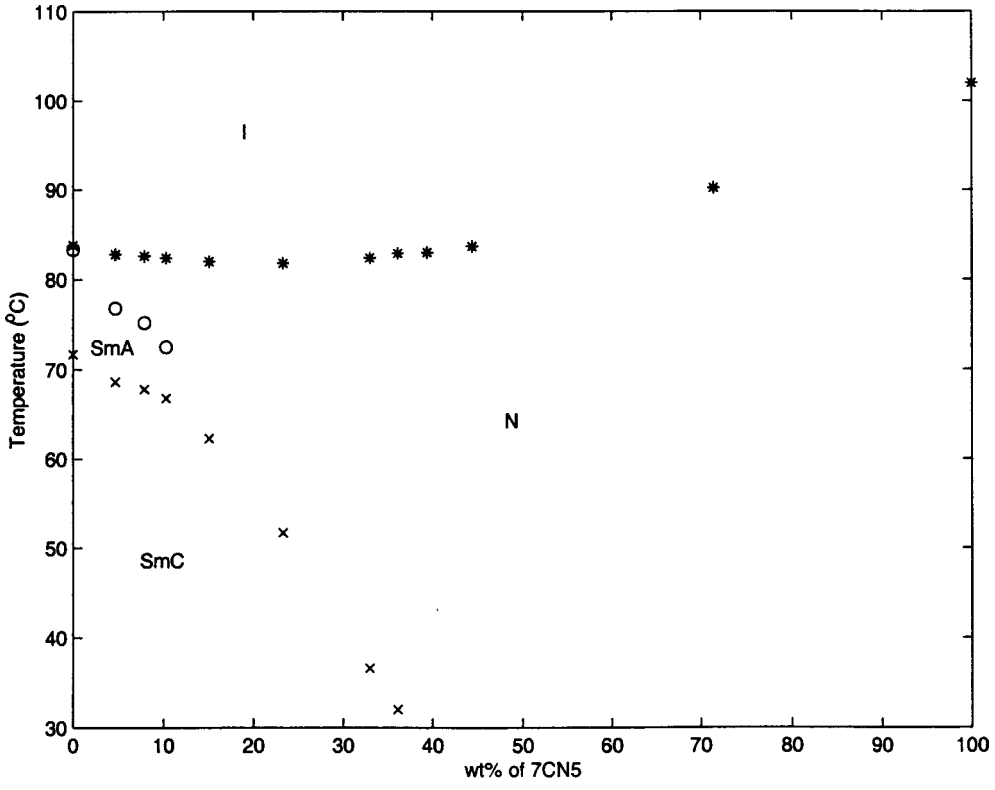

Figure 2.3: Phase diagram of the 70.7–7CN5 mixtures. The transition to the hexatic SmB phase is not shown. The symbols indicate the temperature at which the first domain of the lower temperature phase formed when the sample was cooled.

2.2.1 Sample preparation

The sample cells were constructed using clean indium-tin-oxide (ITO) coated glass plates. The ITO surface was spin-coated with a solution of Polyimide, which is a polymeric compound, and cured at 300^oC. The coated surface was then unidirectionally rubbed using good quality tissue paper. The rubbing action creates parallel grooves on the coated surface. This favours a uniform alignment of the nematic director along the rubbing direction (homogeneous alignment). The plates were then cut to size and the cell assembled using mylar strips of a well defined thickness as spacers and a silicon rubber adhesive. The cell thickness was measured from the interference pattern formed by white light reflecting from the air film inside the cell using a constant deviation spectrometer (Adam and Hilger Ltd.). The cells were filled with the sample in the isotropic phase after thorough mixing, to minimise variations in concentration. Also, 70.7, being a schiff base, degrades easily and hence the cells were hermetically sealed using silicon rubber after filling with the sample.

2.2.2 Growth in cells treated for homogeneous alignment

The observations were made using a Leitz polarising microscope and the sample temperature was controlled by a Mettler FP80 hot-stage which has an accuracy of $\pm 0.1^oC$. The sample, taken in a $35\mu m$ thick cell, was first heated to the isotropic phase and allowed to equilibrate. On cooling to the nematic phase, the nematic aligned homogeneously and hence appeared dark between polarisers which were set parallel and perpendicular to the nematic alignment direction. When the sample was further cooled to about 36.1^oC, SmC domains started nucleating in the nematic phase. These domains had a strikingly different shape and texture compared to the well known broken-focal-conic domains ('bâtonnets') formed by most SmC liquid crystals [23]. They had a *highly anisotropic* shape and always nucleated in the bulk of the sample. As the temperature was lowered the domains grew very rapidly along

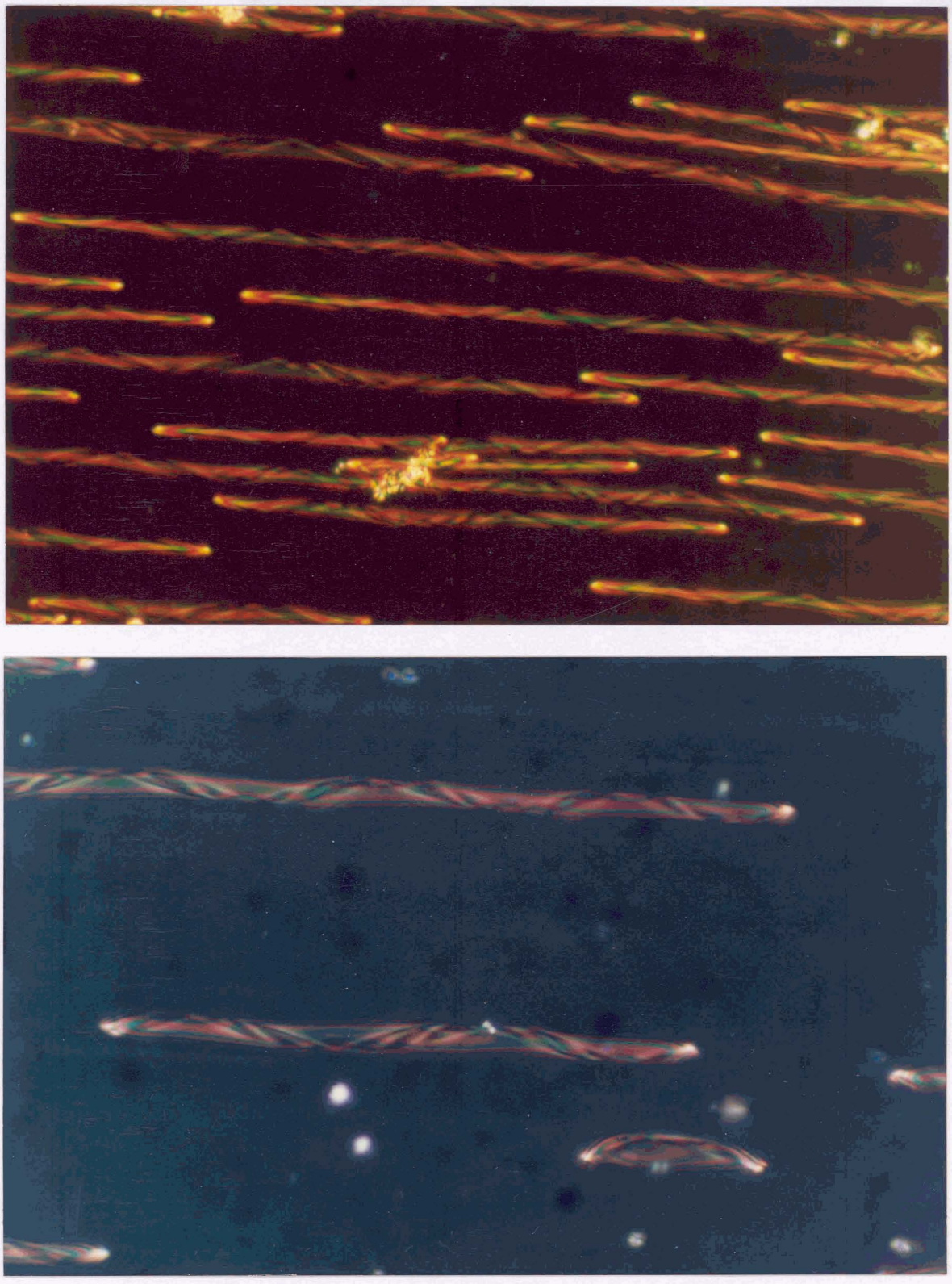

Figure 2.4: Photographs of the chiral domains formed in a $35\mu m$ thick cell treated for homogeneous alignment. (a) Immediately after they were formed and (b) a few domains after they had achieved their equilibrium shapes. The pitch of the helices in both the pictures (which are of different magnifications) is about $90\mu m$ and the domain radius is about $10\mu m$.

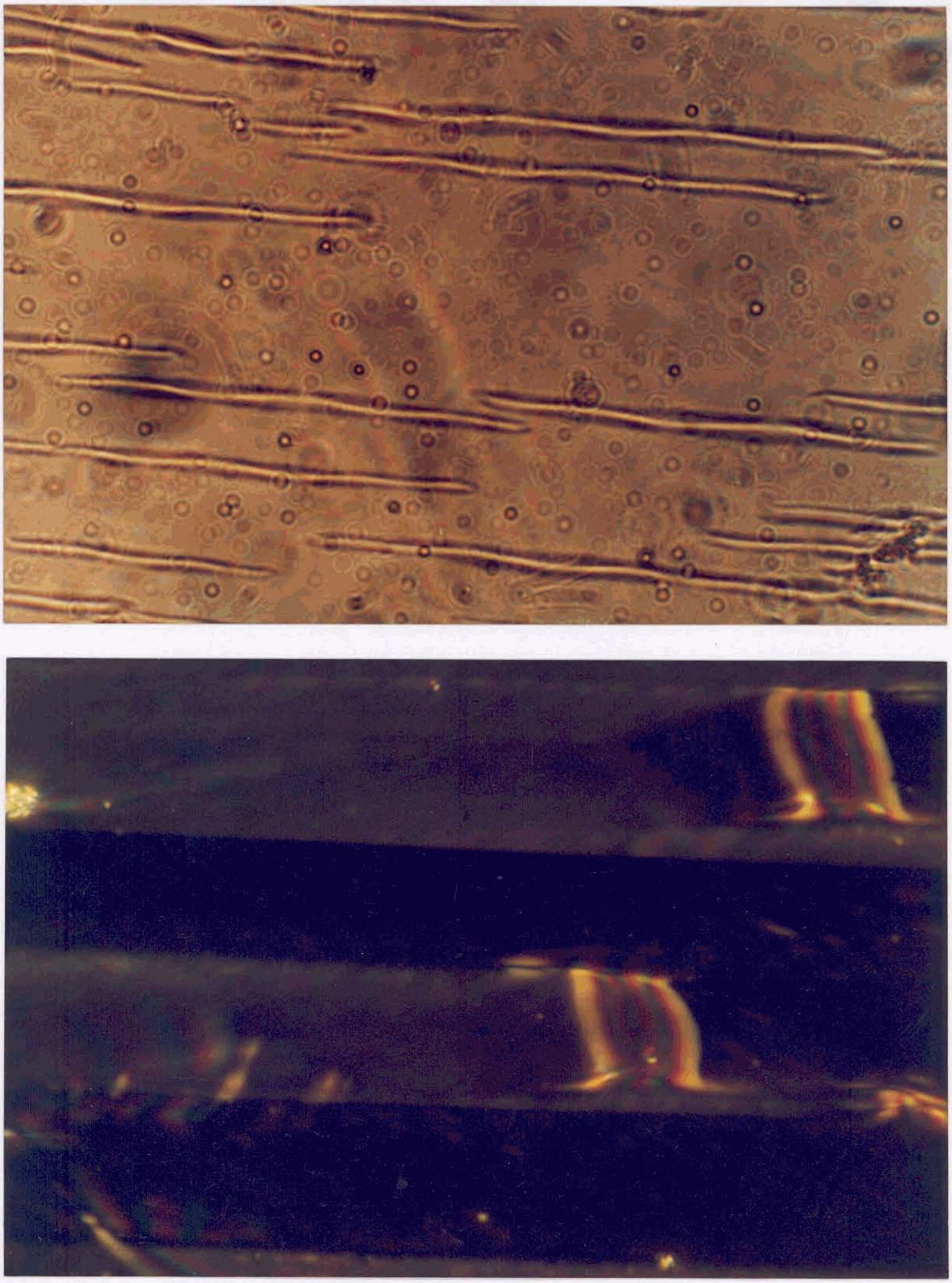

Figure 2.5: (a) The domains with the helical bands viewed without the polarisers. The bright wavy line was found to follow the helix when focussed at different points along the line. (b) Photograph showing the two types of domains that formed when the entire sample transformed to the SmC phase. Adjacent domains had $\hat{\mathbf{n}}$ tilted by a small angle $(\sim 3^o)$ in opposite directions, with respect to the alignment direction. The polariser was set such that one set of domains was crossed out.

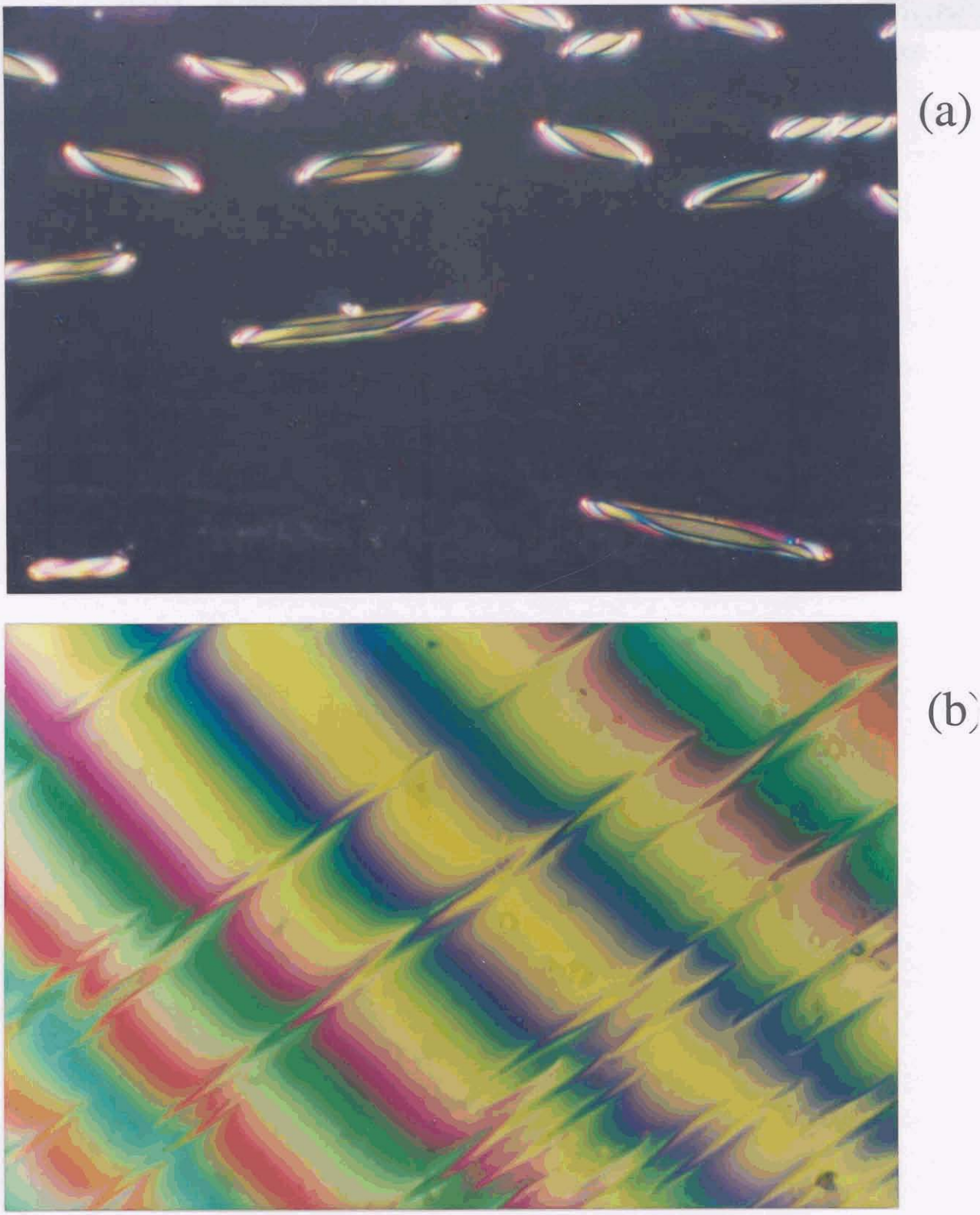

Figure 2.6: (a) Photograph of the unwound domains formed in a $3\mu m$ thick cell. The polariser was set parallel to the nematic alignment direction. The domains were oriented at an angle with respect to this direction. (b) The fringe pattern obtained using a tilting compensator shows the variation of the path difference across the domains, which are oriented at 45^o with respect to the bottom edge of the photograph.

the nematic alignment direction (see Fig. 2.4a). The growth in the perpendicular plane was extremely slow. Thus, the domains formed highly elongated rod-like structures. Domains with very different lengths had roughly the same width. When the temperature was held constant in the coexistence range, the domains attained their equilibrium shape shown in Fig. 2.4b. The domains retain their shape and texture for tens of hours. Between crossed polarisers it was seen that a *helical band* consisting of a few dark and bright stripes was wrapped around each of these domains. The bands terminated at the tips of the domains. The handedness of the helices could be determined by adjusting the focus of the microscope. Roughly equal numbers of both left-handed and right-handed helices were seen. The pitch of the helix depended only on the radius of the domain and decreased towards the tapering tips. In a typical domain, the pitch was $\sim 90\mu m$ near the centre where the domain diameter was $\sim 10\mu m$. On removing the analyser/polariser and refocusing, a bright wavy line could be seen in place of the helical band (see Fig. 2.5a). The region around the helical band acted as a convex lens. Such an effect is usually seen around disclination lines or walls [1, 2, 7] in which there is a rapid variation in the director field close to the defect-line or the wall. This results in a modulation of the effective refractive index and the region focuses light. When the temperature was lowered further, the domains merged and also touched the glass walls of the cell. At this stage, the domains started 'unwinding' and became broad and uniform except near the tips. After the entire sample was transformed to the SmC phase, two types of broad, uniform regions were seen (see Fig. 2.5b). Adjacent strips had $\hat{\mathbf{n}}$ tilted in opposite directions with respect to the surface alignment direction $\hat{\mathbf{a}}$ and were separated by straight, sharp, walls. At either ends of each band colour variations could be seen indicating large distortions in the director field. On slowly *heating* the sample from this state the rod-like domains with the helical bands could be recovered.

In very thin cells ($\sim 4\mu m$), the helical structure spontaneously unwound, presumably when the domains started touching the glass plates which were treated to produce a homogeneous alignment of the director. The unwound domains had a very uniform texture, except near the tips, and they oriented at an angle with respect to the rubbing direction (see Fig. 2.6a). These domains could be crossed out when the polariser was rotated by a few degrees ($\sim 5^o$) away from the domain axis and keeping the analyser in the crossed position. The structure of these 'unwound' domains is similar to that got by the application of an electric field as described in Sec. 2.2.4.

2.2.3 Observations using tilting compensator

In order to determine the structure within the smectic layers we studied the variation of the optical path difference across the domains using a tilting compensator.

The tilting compensator consists of a birefringent plate of uniform thickness which can be rotated about an axis perpendicular to the slow axis (optic axis) of the crystal. The compensator is introduced with its slow axis oriented at 45^o with respect to the crossed polariser and analyser. The path difference introduced between the ordinary and the extraordinary rays can be varied by tilting the compensator plate. Now, if the sample (a homogeneously aligned nematic, say) is placed with its slow axis perpendicular to that of the compensator the net path difference is the difference of the optical paths introduced by the sample and the compensator. Thus, by adjusting the tilt angle it is possible to exactly cancel the path difference introduced by the sample. This path difference can be calculated by measuring the tilt angle of the compensator.

A schematic diagram of the optical set-up is shown in Fig. 2.7. It is important to note that the light, after passing through the sample, is focused by the objective of the microscope and hence is convergent when passing through the compensator.

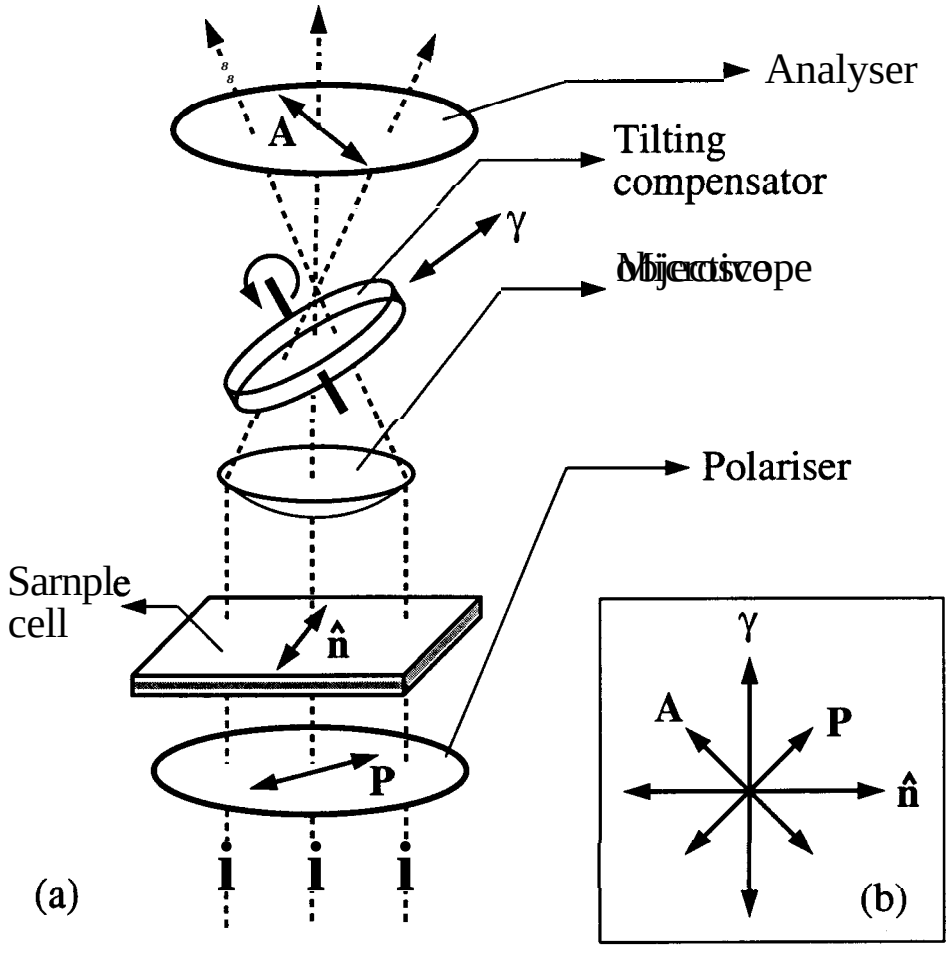

Figure **2.7:** Schematic representation of the tilting compensator set-up. The compensator can be tilted about an axis perpendicular to its slow-axis denoted by γ. The inset shows the relative orientations of the various components.

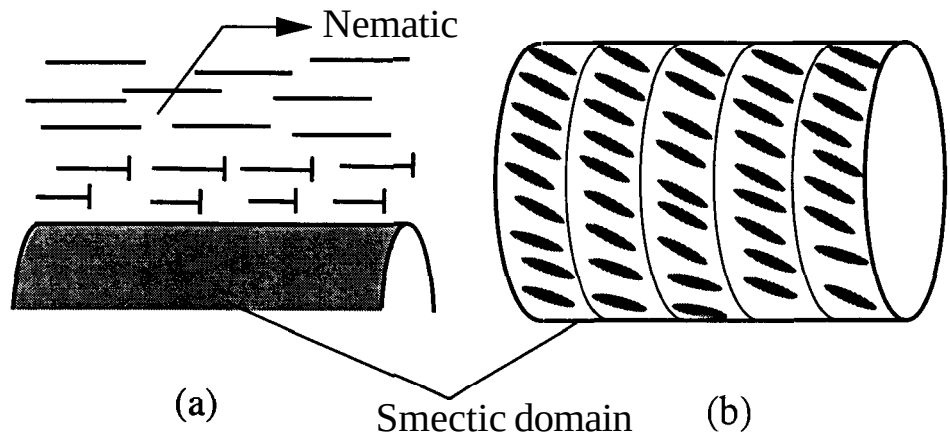

Figure 2.8: (a) A schematic of the twist deformation in the nematic close to the *N-SmC* interface. The nails represent the projection of the director with the nail-head indicating the end which is projecting out of the plane of the paper. (b) Shows the arrangement of the molecules within the *SmC* domain and close to the *N-SmC* interface.

Because of this, compensation can be achieved only along a line (which usually appears as a dark band) and not over the entire sample. Bands of varying colours appear on either sides of the dark one. Therefore, for making quantitative measurements, only the central region where the rays are paraxial should be considered. However, the deformations in the fringe pattern gives a qualitative picture of the relative variations in the path difference across the sample.

In our experiments, in the nematic phase, the fringes were straight and uniform, as expected. When the *SmC* domains formed, the fringes showed sharp variations across each domain. The path difference decreased continuously as the *SmC* domain was approached, reached a minimum at the interface, and then increased rapidly to a maximum value at the centre of the helical band (see Fig. 2.6b). The sharp increase within the domain followed the helix when the sample was moved continuously along the domain axis. This supports the earlier argument that there is a sharp variation in the effective refractive index close to the helical band. Note that in the absence of the compensator the nematic close to the domains, as well as the rest of the nematic, appeared dark between crossed polarisers, when the alignment direction was along

one of the polarisers. Therefore, the path difference variation in the nematic near the domains indicates that the director-field close to the domains is distorted such that the *projection* of $\hat{\mathbf{n}}$ on to the plane of the cell is everywhere oriented along the rubbing direction. Such a deformation will not affect the state of polarisation when the polariser is set along the rubbing direction and hence appears dark when the analyser is kept in the crossed position. But since the director, which is also the optic axis, is tilted with respect to the ray propagation direction, there is a reduction in the optical path difference introduced when the polariser is set at an arbitrary angle with respect to the rubbing direction. This was reflected in the fringe pattern obtained in the compensator experiment. Thus, there is an almost pure *twist deformation* in the nematic director field as shown in Fig. 2.8a. Also, the continuity of the fringes across the *N-SmC* interface indicates that the Frank-director within the smectic domain was tangential to the interface and was *tilted* with respect to the domain axis as shown in Fig. 2.8b.

2.2.4 Electric field experiments

Both the components of the mixture have negative dielectric anisotropies. Therefore, under the action of a uniform electric field the molecules would prefer to lie in a plane perpendicular to the field direction [1, 2]. Since static or low frequency alternating fields produce unwanted effects like electrohydrodynamic motion [1, 2] and heating of the sample due to the motion of ionic impurities, a high frequency $(10KHz)$ field was used. Such an electric field applied between the ITO coated plates had the following effects on the SmC domains. As the field strength was increased the helical structure of the domains started 'unwinding'. At a high enough field the domains were fully unwound (see Fig. 2.9). When this happened the domains also appeared considerably wider compared to the field free case. No change in their lengths was noticed. This means that the domains had become flattened, assuming that their volumes remained the same.

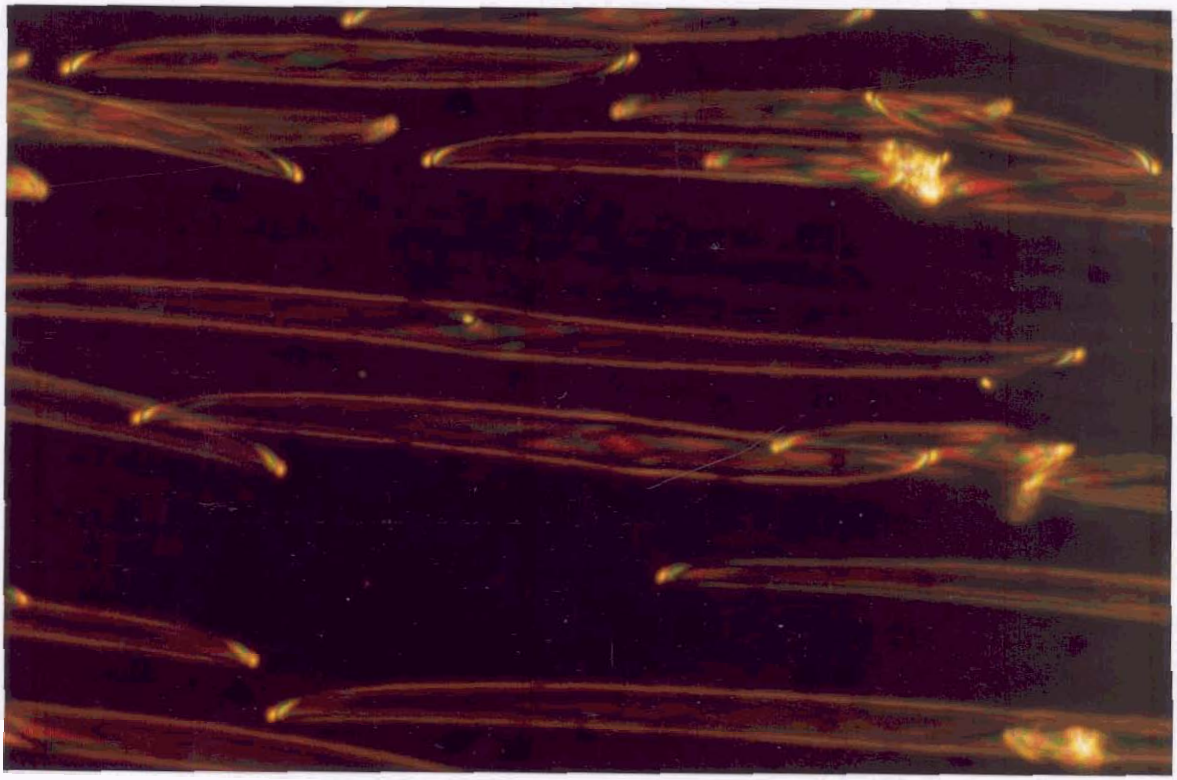

Figure 2.9: Photograph of the more or less uniform domains obtained by applying an alternating electric field of $\sim 3V/\mu m$ across the ITO coated glass plates. Note that the domains have become broad and more or less uniform compared to those in Fig. 2.4b, which were recorded with the same magnification.

Two distinct sets of domains could be seen. The two sets were rotated by equal and opposite angles with respect to the nematic alignment direction. This angle was approximately equal to the SmC tilt angle at the same temperature. The domains could now be almost completely crossed out, one set at a time, when the sample-stage was rotated by about 3^o in either direction. Now when the tilting compensator was introduced the path difference was seen to be more or less uniform across the domains, except near the tips. The director distribution in a uniform portion of the flattened domains is shown in Fig. 2.10.

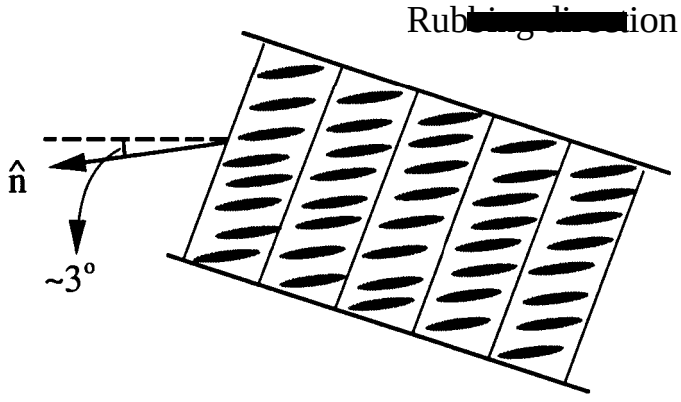

Figure 2.10: A schematic representation of the arrangement of the molecules within a uniform portion of the 'flattened' domains. Note that the orientation of the Frank-director within the domain is roughly the same as that of the nematic outside, indicated by the double-headed arrow.

The fact that the flattened domains oriented themselves at an angle shows that the interfacial tension at the N-SmC interface was a minimum when the Frank-director had the same orientation on either sides of the interface, as might be expected. In the flattened domains this could be achieved without causing any distortion in the nematic between the glass plates and the domains by orienting the the latter at an appropriate angle with respect to the nematic alignment direction. When the field was switched off, the domains regained their original structure in about half an hour. This observation and the fact that these domains can be obtained on heating as well as on cooling proves that these domains are indeed

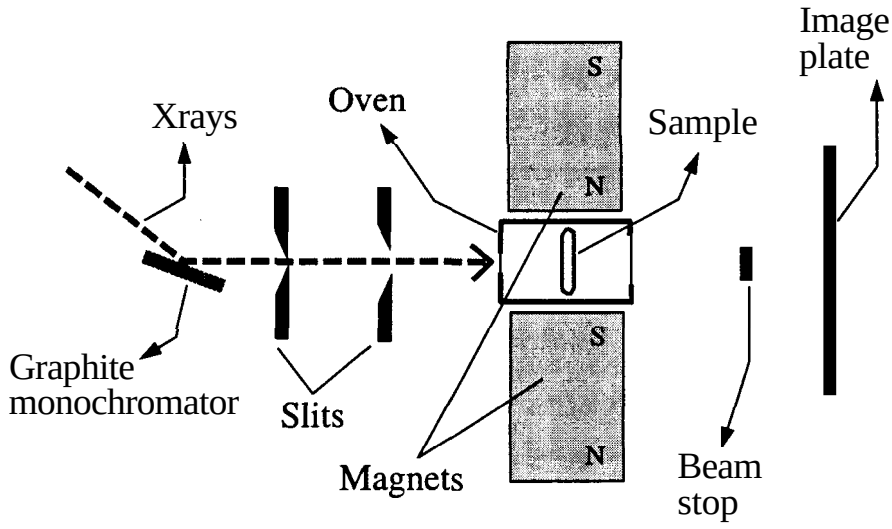

Figure 2.11: A schematic diagram showing the set-up for the xray experiments on the magnetically aligned samples. The sample alignment is along the direction of the field.

equilibrium structures.

2.2.5 Xray diffraction studies

Xray diffraction studies were conducted using both magnetically aligned and surface aligned samples. In the first case, the sample was taken in a $0.5mm$ Lindemann capillary tube whose ends were flame-sealed. The oven used for controlling the sample temperature, was equipped with a pair of ceramic magnets which generated a field of about $6kG$ along the length of the capillary. This oven was specially constructed for xray experiments using aligned samples and the details of it are given in Sec. 2.4. Both the components of the mixture have a positive diamagnetic susceptibility anisotropy $(\chi_{\|} - \chi_{\perp})$ and hence the molecules tend to align along the direction of the field [1, 2]. A graphite monochromator was used to select $Cu\text{-}K_{\alpha}$ radiation produced by a fixed tube generator (Enraf). The beam was collimated using a double slit arrangement. The beam was sent normal to the magnetic field. The diffraction patterns were recorded on an image plate procured from Marresearch. A schematic diagram of the experimental arrangement is shown in Fig. 2.11. The

patterns obtained at different sample temperatures are shown in Fig. 2.12.

The diffraction pattern from the nematic phase clearly shows four intensity maxima (see Fig. 2.12a). The radial intensity distributions across the peaks are sharper than what is usually seen for ordinary nematics. This pattern with four intensity maxima is characteristic of a nematic with skew-cybotactic order [1]. A schematic diagram of the SmC-like short-range order in the nematic is shown in Fig. 2.13a. Each pair of the diffraction peaks (which are diagonally oriented) corresponds to one set of smectic layers which are appropriately oriented. The average molecular length calculated from the distance between each set of peaks and the angle between the two pairs is 28.7^oC. The tilt angle in these SmC-like groups is 30" at 34.5^oC. On cooling the sample to just below the N-SmC transition point four sharp spots appear in addition to the nematic peaks (Fig. 2.12b). These spots occur at a slightly larger **q** compared to those from the nematic. These four sharp peaks correspond to the SmC domains. At 32.5^oC, the tilt angle in the cybotactic groups is 28^o and that in the smectic domains is 30^o. These values were calculated from the layer spacing measurements, assuming the same value for the average molecular lengths in both the coexisting phases. A direct measurement of half the angle between the two pairs of peaks from each medium will give the angle by which the layer normal is tilted with respect to the field direction (see Fig. 2.13). In the cybotactic nematic, the short-range layer order makes an angle of 28" with respect to the field (see Fig. 2.13a). This value is equal to the tilt angle calculated from the layer spacing. This means that the directors within the SmC-like groups are parallel to the field. In the case of the SmC domains, however, the half-angle between the two sets of peaks corresponding to two different orientations of the layers is only 11^o. This is much smaller than the tilt angle calculated from the layer spacing. This probably means that the director within the smectic domains have not fully oriented along the field direction. As the temperature is further lowered the SmC peaks become

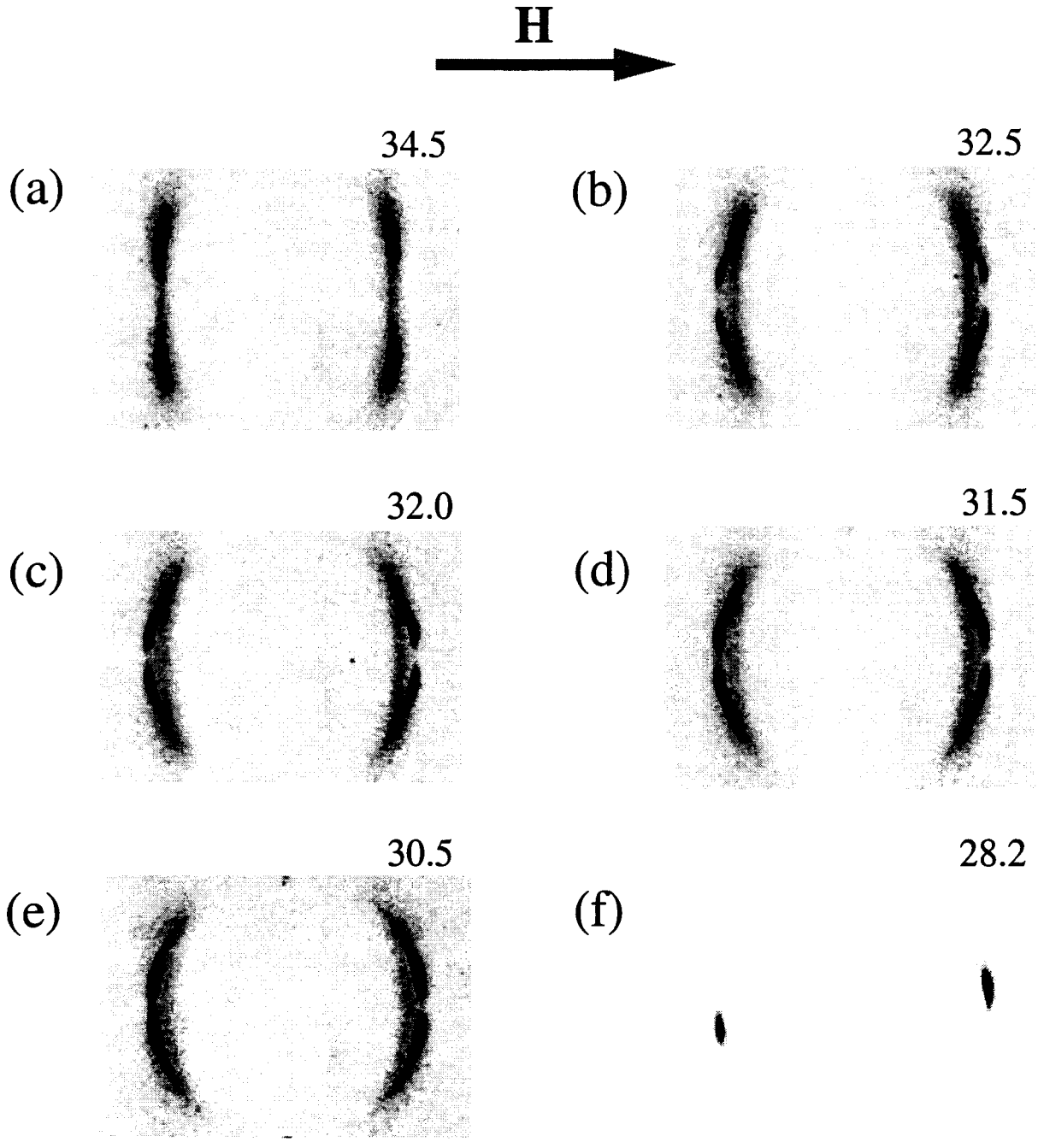

Figure *2.12:* The xray diffraction patterns obtained from a magnetically aligned sample, a mixture with $36.0wt\%$ $7CN5$, at various temperatures. The sample was cooled in steps of 0.1^oC and held at each temperature for about $15min$ before starting the exposures. The field was applied along the horizontal direction. The last picture (f) was recorded after leaving the sample at 28.2^oC for about eight hours.

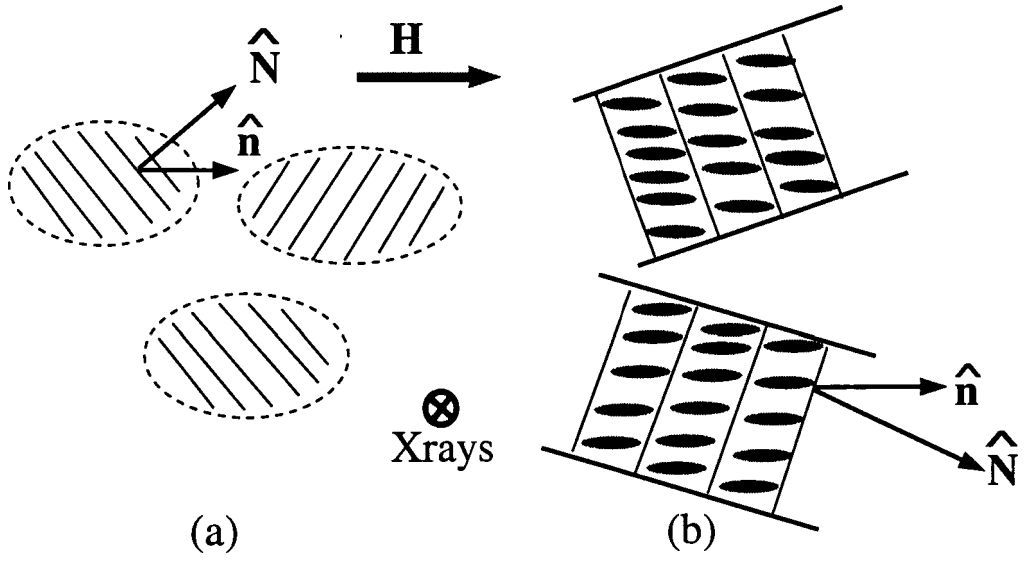

Figure 2.13: Schematics of (a) skew-cybotactic groups in a magnetically aligned nematic. (b) Smectic layering in the domains if the molecules were aligned along the field. Experiments show that the angle made by the layer normal with the field direction is smaller than the tilt angle indicating that the orientation is not as perfect as shown here. In both (a) and (b) the average distribution of the layers is cylindrically symmetric about the direction of the field.

---

more intense and those from the cybotactic nematic become progressively weaker. Also, the q-vector of the SmC diffractionspots increases in magnitude. On leaving the sample overnight $(\sim 8hrs)$, at a low enough temperature so that the transition to the SmC phase is complete, only two very intense peaks, corresponding to a monodomain SmC phase, are seen (Fig. 2.12f).

Since the magnetic field tends to align the molecules and hence the smectic layers within the SmC domains as well as those of the nematic, the patterns in Fig. 2.12 do not correspond to the field-free structure described in Sec. 2.2.2. In order to determine the orientation of the SmC layers within the domains in the absence of any external fields, the experiment was repeated using a surface aligned sample. For this a cell was constructed using $\sim 30\mu m$ thick glass plates obtained by etching one side of cover slips (see Fig. 2.14a). The smooth surface was then coated with SiO at oblique incidence for homogeneous alignment [30]. The cell thickness

Figure 2.14: (a) A schematic diagram of the cell constructed using etched cover-slips. (b) The diffraction pattern obtained from a $31.6wt\%$ $7CN5$ mixture taken in a treated cell at a temperature of 34.9^oC. The overall rotation of the pattern is due to the orientation of the alignment direction not being exactly along the horizontal direction. The pattern from the nematic appear as four bright patches, whereas, that from the SmC domains appear as arcs. Note that the intensity is distributed symmetrically about the preferred alignment direction.

---

was fixed at $\sim 15\mu m$. The temperature was controlled using a Mettler $FP80$ hot-stage with mylar windows. The temperature was lowered from the nematic phase into the coexistence region. The alignment of the nematic was checked using a microscope before exposing the sample to the xrays. The incident beam was normal to the alignment direction. The pattern obtained after an exposure of four hours is shown in Fig. 2.14b. Compared to the magnetically aligned sample, the intensity distribution of the diffraction pattern from the smectic domains is more or less symmetric about the equatorial direction which is also the alignment direction. The wide diffraction arcs might arise because of the presence of a few domains which are unwound due to the interaction with the treated plates of the thin cell as was discussed in Sec. 2.2.2.

2.2.6 Discussion on the domain structure

The xray experiments indicate that the SmC layering is, on the average, perpendicular to the domain axis. The optical experiments using a tilting compensator indicate that at the surface of the domains the local Frank-director lies in the tan-

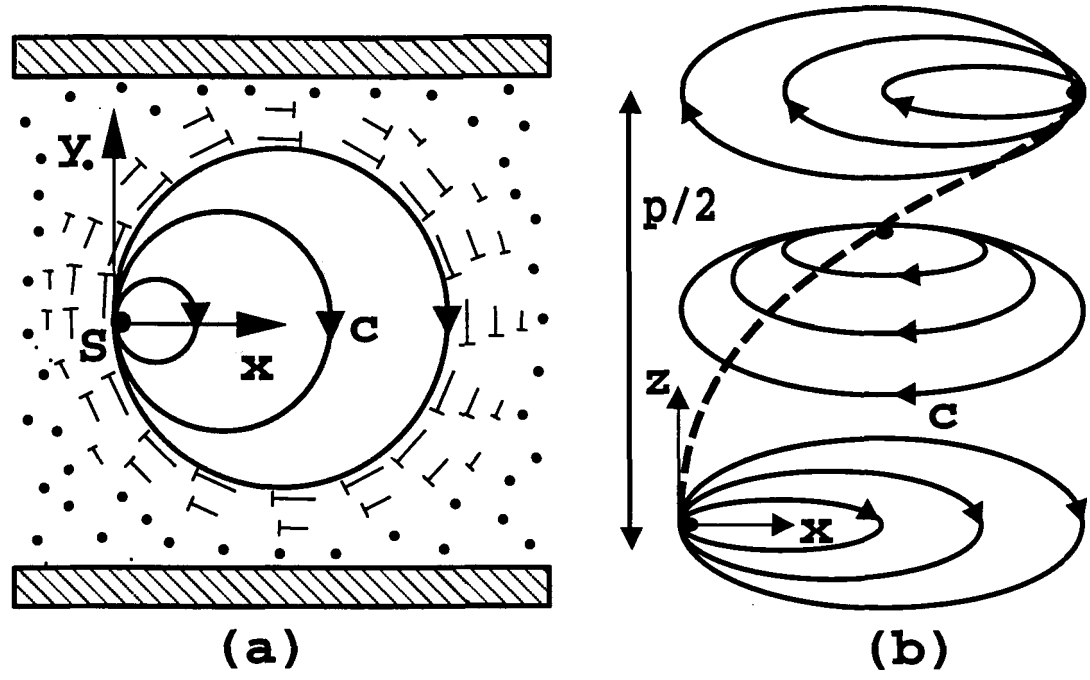

Figure 2.15: (a) The circles represent the c-field within a SmC layer (shaded region). The point S is a singularity. The nails represent the projection of the $\hat{\mathbf{n}}$-field of the nematic around thedomain with the heads indicating the end that projects above the plane of the paper. At the glass surfaces, the nematic director is aligned normal to the plane of the diagram. (b) The c-field in a few representative layers within half a pitch p of the structure. The pattern in (a) rotates from layer to layer. The dashed line is the locus of S.

---

gent plane and is tilted by an angle equal to the SmC tilt angle with respect to the domain axis. With such an alignment on the boundary, topological considerations demand the existence of a singularity in the c-field within each layer. The director field and hence the effective refractive index can be expected to vary rapidly close to this singular point. The path difference measurements and the focusing effect seen in the absence of the polarisers indicate that such a rapid variation of the effective refractive index occurs close to a helical line wound around the surface of the domain. Based on these experiments described in the earlier sections, we propose the structure shown in Fig. 2.15 for the SmC domains. Within each layer the c-field, which is the projection of $\hat{\mathbf{n}}$ on to the plane of the layers, follows circles of different radii; all the circles pass through the point defect S lying on the surface (Fig. 2.15a).

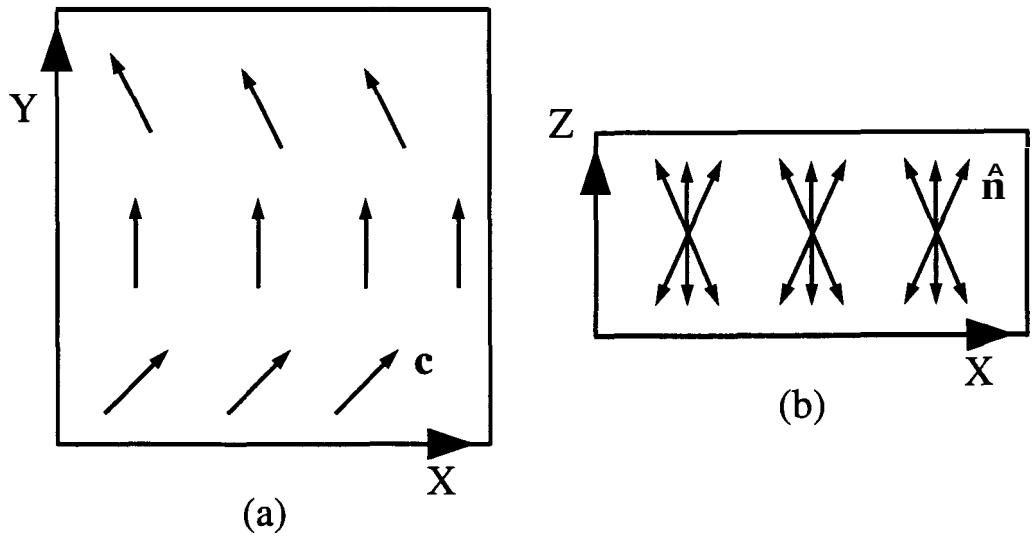

Figure 2.16: (a) A schematic representation of a bent c-vector field in a SmC layer whose layer normal is along the Z axis. (b) A side view of the distortion shown in (a) reveals the twist deformation in the $\hat{\mathbf{n}}$ field.

This c-field configuration within each layer resembles the pattern seen in $2D$ SmI domains of a chiral compound and can be considered as part of a $+2$ disclination [31]. The SmI phase has a tilted hexatic order within the smectic layers [1, 2]. The $2D$ domains were formed in thin free-standing films on cooling the sample from the SmC phase. The $3D$ domain can be visualised as a stack of these layers such that the locus of S describes a helical line that wraps around the cylinder as shown in Fig. 2.15b. Unlike the SmI domains, these $3D$ domains are made of non-chiral molecules.

In the case of the SmI domains the singularity was 'expelled' from the domain by violating the boundary alignment condition over some region. This could be easily seen as the viewing direction was perpendicular to the layers. In the present case it is difficult to say whether the disclination line was expelled or not because the layers are seen edge on.

Clearly, these SmC domains break the chiral symmetry. Each layer with the above mentioned structure lacks mirror symmetry and hence is by itself a chiral

object. The helical structure is formed by a regular stacking of such chiral layers. A more formal discussion of the chiral nature of the domains is as follows. With $\hat{\mathbf{n}} = c + \sqrt{(1 - c^2)}\,N$, where N is the smectic layer normal, it is easy to see that c x (V x c) $\neq 0$ implies $\hat{\mathbf{n}} \cdot (V \times \hat{\mathbf{n}}) \neq 0$. A bend in the c-field necessarily generates a twist in the $\hat{\mathbf{n}}$-field. This is pictorally shown in Fig. 2.16. The curl of $\hat{\mathbf{n}}$ has components both in the plane of the layers and along N. Thus, a bent c-field removes the N-c mirror plane locally [17]. Since the sign of the bend is the same everywhere inside a domain, the chiral symmetry is broken on a macroscopic scale as well. Since this symmetry breaking is spontaneous, both right-handed and left-handed structures form with equal probability.

The $\hat{\mathbf{n}}$-field in the surrounding nematic has a twist distortion as shown in Fig. 2.15a. This is due to the different boundary conditions that have to be satisfied at the glass plates and at the the domain surface. At the cell walls and also far away from the domains the nematic director prefers to be along the rubbing direction. At the surface of the domain the director prefers to align at an angle, which is equal to the SmC tilt angle, with respect to the domain axis. These two conditions can be satisfied by producing a twist deformation in the nematic surrounding the domain. The net torque acting on the domain due to this distortion becomes zero when the domain is oriented along the nematic alignment direction. ie, when the twist distortions in the nematic above and below the domain are equal and opposite. This is why all the domains are always oriented along the rubbing direction.

In the very thin cells, the domains start touching the glass plates when their diameters become larger that the cell thickness. Since the plates are treated to produce a uniform alignment of the director, the structure within the domains get unwoung in order to satisfy this boundary alignment (see Sec. 2.2.2). A similar effect occurs when an external electric field is applied to align the director in planes normal to the field (see Sec. 2.2.4). The exact process by which the domains unwind

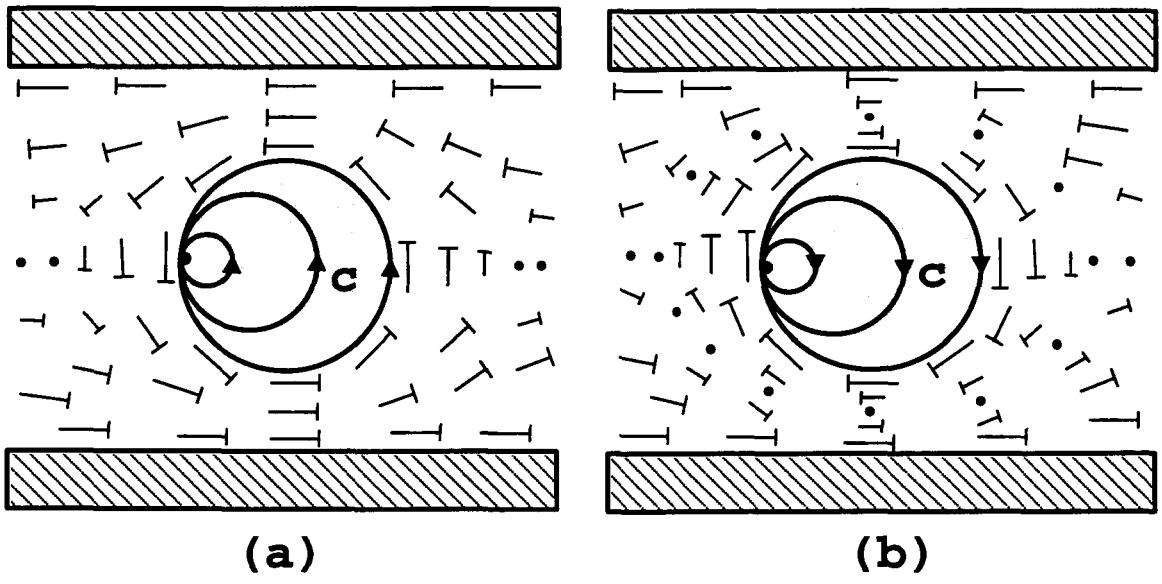

Figure 2.17: Schematic representation of the distortion produced in the nematic by domains with opposite c-fields in a twisted-nematic cell. The nails have the same meaning as in Fig. 2.15. As the distortion in the nematic is much smaller in (a) as compared to that in (b), the former type of SmC domain is favoured.

is not clear.

2.2.7 Growth in twisted-nematic cells

The sense of the c-field within the layers can in principle be different from that of the helical disclination line. Therefore, in order to determine the sense of the c-field, the growth experiments were repeated using cells which produce a twist deformation in the nematic (twisted-nematic cells). This can be achieved by rubbing the two plates of the cell in different directions. In such a cell the domains with right and left handedness of their c-fields will produce very different distortions in the surrounding nematic (Fig. 2.17). In one case the distortion is less compared to the parallel rubbed case whereas for the other it is enhanced. This favours the formation of only one type of domains. Indeed, in the experiments, an imposed twist of 15^o in a $14\mu m$ thick cell produced a yield of about 90% of one type of domains. The helical band was always found to have the same sense of rotation as the c-field in

each domain. This simple experiment also demonstrates the effect of a chiral bias field in producing chiral discrimination. The chiral selection in this case can be easily understood unlike in the sodium chlorate experiment described in reference [14].

2.2.8 Nucleation and growth near a nematic-air interface

The nucleation and growth of the SmC domains at a nematic air interface showed some interesting features (see Fig. 2.18). The domains nucleated as a thin strip, which appeared bright against the dark background, along the interface. As the temperature was lowered, at a rate of $0.1^oC/min$, a periodicity developed along the strip and the N-SmC interface became corrugated. On further lowering of the temperature, the amplitude of the corrugation increased and finally formed periodic finger-like structures. These fingers had an optical texture identical to the domains in the bulk, with the helical band. When the interface was oriented perpendicular to the alignment direction, the fingers grew along the undistorted nematic director. For an arbitrary orientation of the interface, the fingers started off normal to the interface and then slowly curved towards the nematic orientation direction. This is because the energy cost for deformations in the nematic is least when the fingers are oriented along the undistorted nematic director.

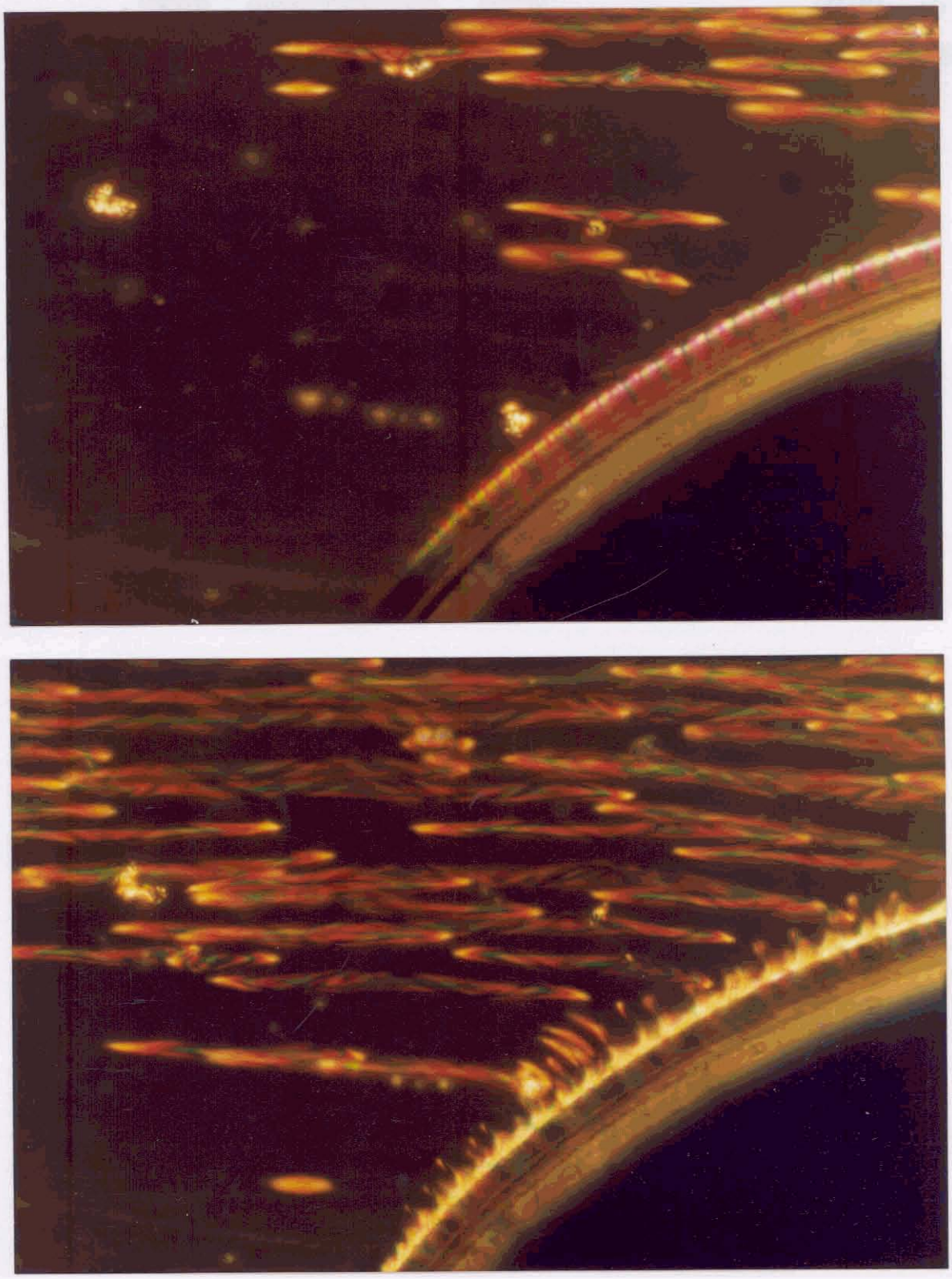

Figure 2.18: Sequence of photographs showing the nucleation and growth of the SmC phase near an air bubble.

2.2.9 Domain formation in cells of different thicknesses

Experiments on cells having different spacings between the glass plates showed that the diameter of the domains varied with the cell thickness. Measurements were made on five cells with thicknesses ranging from about 4pm to $235\mu m$. Thicknesses below $\sim 100\mu m$ were measured using the interference technique (Sec. 2.2.1) to an accuracy of better than ± 0.1pm. The cell thickness varied by about ± 1pm. Larger thicknesses were measured using the microscope by focussing on scratches or dust particles at the two treated surfaces of the cell. The distance could be read off the graduated focussing drum of the microscope which had a least count of $1\mu m$. The variation in thickness was around $\pm 5\mu m$.

All the cells were filled with the same mixture in the isotropic phase and the cells were then sealed using silicon rubber adhesive. The cells were maintained at around 40^oC in an oven so that the mixture always remained in the nematic phase. For making the measurements each cell was transferred to the Mettler hot-stage without allowing it to cool into the N-SmC coexistence range. The temperature was then lowered at a rate of $0.1^o/min$.

It was noticed that the temperature at which the N-SmC transition started reduced with reduction in cell thickness. The variation of the N-SmC transition temperature as a function of the cell thickness for two independent sets of cells and mixtures are shown in Fig. 2.19. In order to confirm that the variation is not just due to concentration differences, the transition was studied in wedge-shaped cells. The wedge shaped cells were constructed by assembling the two treated plates such that the top plate was in contact with the bottom plate along one edge and was separated by a mylar spacer at the opposite edge. The preferred alignment direction was along the lines of equal thickness. In such cells, when the mixture was cooled from the nematic phase, the SmC domains always started nucleating from the thickest end of the cell. A comparison of the transition temperatures at different thicknesses was

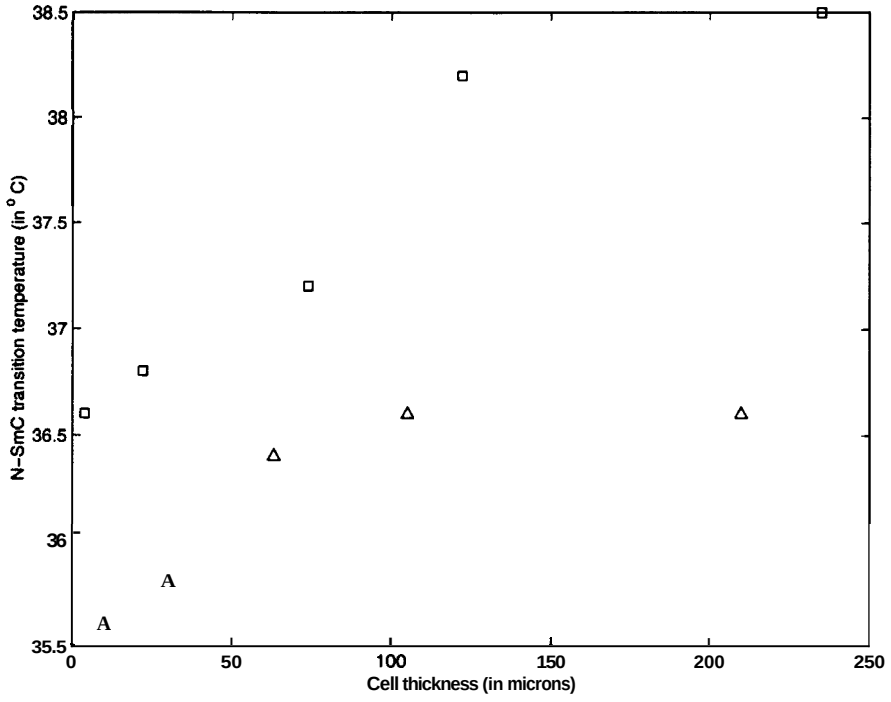

Figure 2.19: Variation of the N-SmC transition temperature as a function of the cell thickness. The temperatures correspond to that at which the first SmC domain appeared on cooling from the isotropic phase at a rate of O.l°/min. The different symbols correspond to different mixtures of slightly different compositions.

not possible in this case as the composition of the remaining nematic varied as more and more of the material was transformed into the SmC phase.

The reduction in the transition temperature could be due to the twist deformation that occurs in the nematic when the SmC domains are nucleated. The orientation of the nematic director varies by an angle 8, which is the SmC tilt angle, on going from the treated plates of the cell to the surface of the domain. When the radius of the domain is very small compared to the cell thickness, the average twist in the nematic can be written as $((\mathrm{V} \times \mathrm{fi})) = 2\theta/d$, where d is the cell thickness. By a simple dimensional analysis [32, 33], the transition temperature, T', in a cell of finite thickness can be related to that in the absence of any twist distortion, T^o, by the equation

$$T' = T^o - lT^o|(\boldsymbol{\nabla} \times \hat{\mathbf{n}})|. \tag{2.1}$$

Using typical values, $T^o = 300K$, 8 = $0.2rad$, d = 4pm and $T^o - T' = 1K$ (see Fig. 2.19), we get $l \simeq 300\mathring{A}$. This value of l is about ten times the molecular length

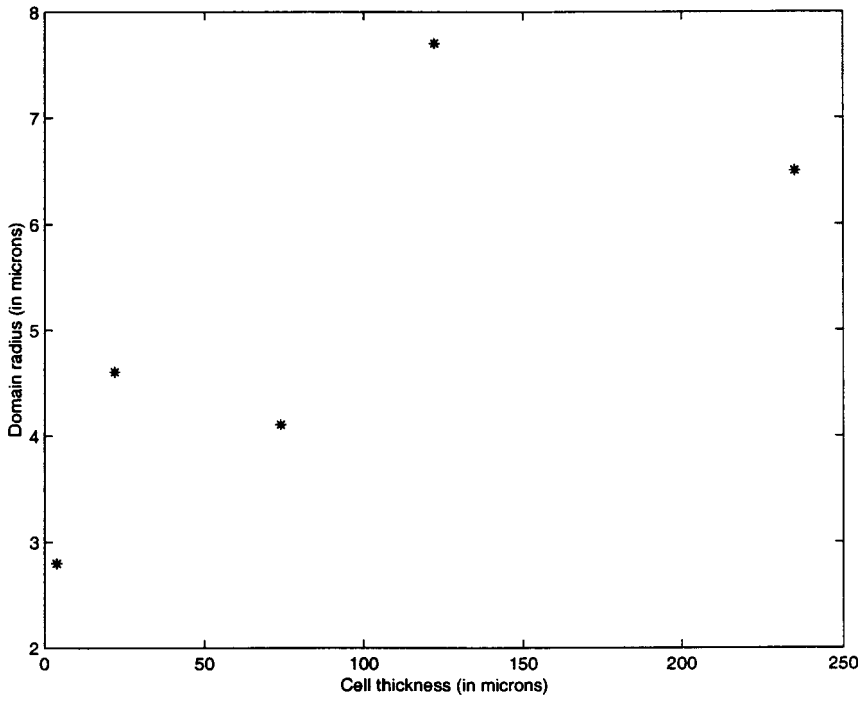

Figure 2.20: Plot of the radius of the domains in cells of different thicknesses. Each point is an average of several domains of different lengths that formed in a given cell.

and might correspond to the average size of the cybotactic groups which have a strong SmC-like short-range order as seen in the xray pattern shown in Fig. 2.12a.

For making measurements on the domains in cells of different thicknesses, the sample was cooled to 0.1^oC below the temperature at which the first domain appeared and was held at that temperature for about half an hour to allow the sample to equilibrate. The microscopic images of the domains were then recorded on a videotape using a CCD camera. Measurements were made on the recordings using a Data Translation high resolution frame grabber system. The pixel size was calibrated for each magnification using a Leitz micro-meter scale. The pixel size was $0.38\mu m$ along the horizontal and $0.26\mu m$ along the vertical direction at $\times 250$ magnification, which was used for most of the measurements.

A plot of the domain radius, averaged over several domains of very different lengths in each cell, as a function of the cell thickness is shown in Fig. 2.20. The radius of the domains increases with the cell thickness. This dependence on the cell thickness probably indicates that the surrounding nematic plays a crucial role in

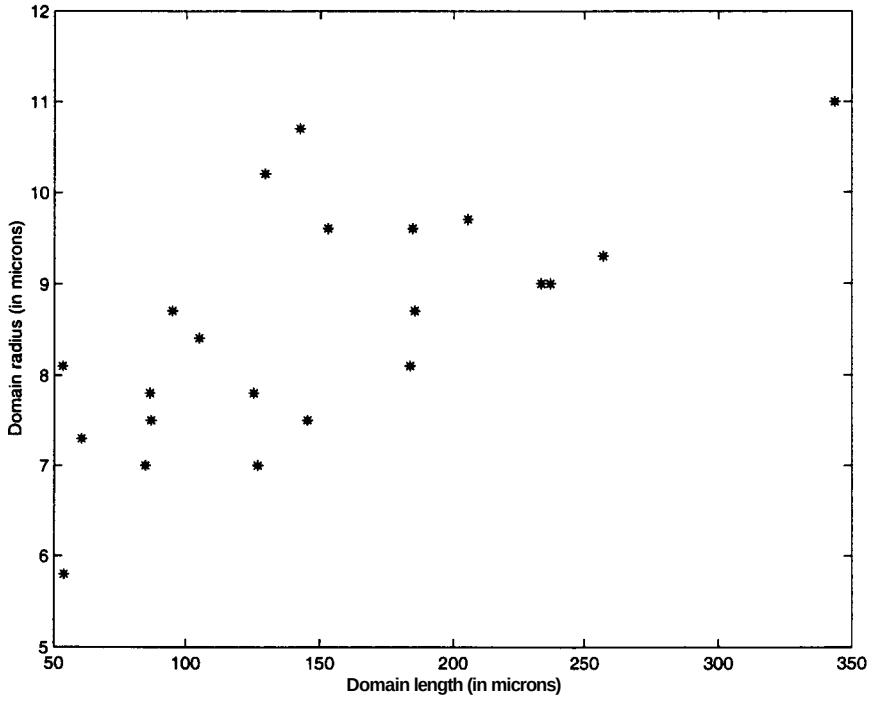

Figure 2.21: Plot showing the increase in radius with length of the domains.

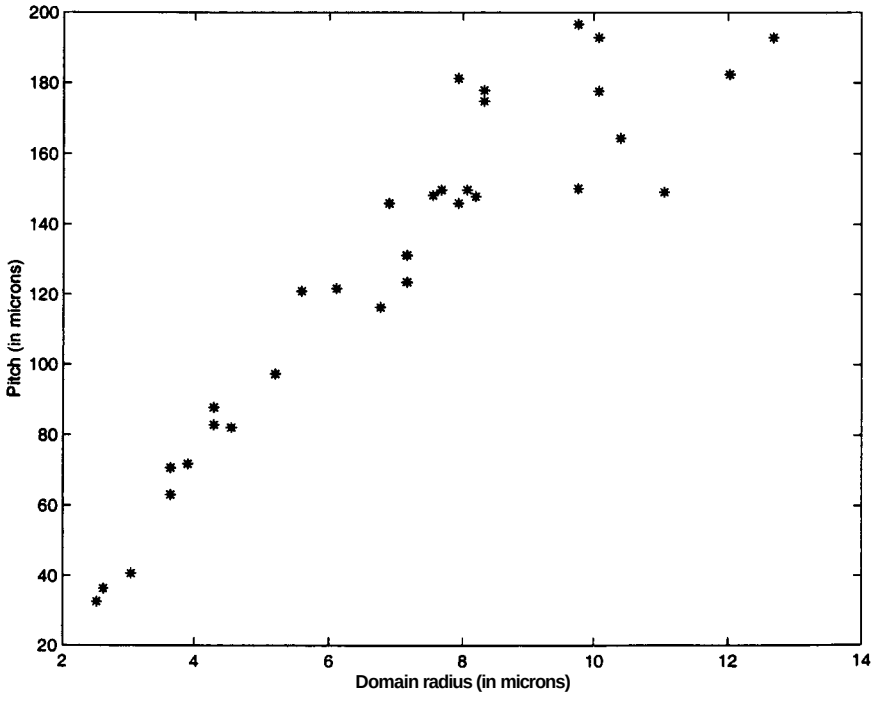

Figure **2.22:** Variation of the pitch of the helix as a function of the domain radius. The measurements were made from cells of different thicknesses. Only domains which were long compared to the pitch were chosen for making the measurements.

determining the shape of the domains. Even in the same cell, there was a gradual increase in the radius with the length of the domain as shown in Fig. 2.21.

The helical pitch was seen to be roughly proportional to the domain radius. The dependence of the pitch of the helix on the domain radius is shown in Fig. **2.22.** The measurements were made on several domains formed in cells of different thicknesses. Only domains which were several pitches long were chosen for the measurements.

2.3 Conclusion

In conclusion, we have studied a new type of chiral structure formed by smectic-C domains nucleated from the nematic phase of a binary mixture. This is the first example of the formation of such a periodic helical structure formed by three-dimensional domains of an achiral SmC liquid crystal. The chirality of the domains could be selected by imposing a simple twist deformation in the surrounding nematic. The mechanism for this chiral discrimination could be easily explained unlike in the case of crystals [14].

These domains also exhibited very unusual growth patterns. The dependence of the domain radius on the cell thickness indicates that the distortion produced in the surrounding nematic plays an important role in determining the domain shape. The large coexistence range shown by the binary mixture made the study of the equilibrium structure and shape of these domains convenient.

In the next chapter we present a theoretical analysis which explains the stability of the helical structure and the unusual shape exhibited by these domains.

Appendix

2.4 Construction of the oven and controller for xray experiments

The xray experiments described earlier in this chapter required an oven with excellent temperature stability and a provision for applying a strong magnetic field for aligning the samples. In this section we describe the construction of such an oven and its control system.

2.4.1 Essentials for good temperature control

The performance of a temperature control system depends on the optimisation of a number of factors. Some of these are listed below.

- An optimum thermal mass and insulation should be chosen. A very small thermal mass or less insulation will make the oven temperature fluctuate easily with the ambient temperature. On the other hand, too high a thermal mass or too much of insulation will make the oven 'sluggish' to temperature corrections.

- The maximum input power available should be roughly twice the steady-state power requirement. This ensures that the temperature can be raised quickly when it falls below the target temperature. Also, the steady state power should be large enough so that the oven can be cooled quickly by reducing the input power.

- The heating element and the sensor should be very well coupled to the load.

Also, the coupling between the heating element or the sensor to the load should be better than that between the heating element and the sensor.

- The sensor should be placed as close to the heating element as possible in order to reduce the response time. To achieve this and the previous condition , the sensor is placed inside the heater block but very close to the heating eleme nt.

- The heating elements should be symmetrically distributed to reduce temperature gradients.

2.4.2 The principle of a PID controller

The simplest temperature controller is one in which the input power is simply proportional to the difference between the target temperature and the heater temperature, $\Delta(t) = T_{target}(t) - T_{heater}(t)$, at any given time t. The output power is then

$$W(t) = P\Delta(t) \,. \tag{2.2}$$

But in such a system the input power goes to zero as the heater temperature approaches the target temperature. This leads to an oscillatory behaviour. In order to overcome this problem, a second part is added to the input power. This quantity is proportional to the temperature difference $\Delta(t)$ integrated over time. When the target temperature is reached, this will be a non-zero value even though the temperature difference is zero. If the heater response has to be fast the proportional term should be made larger. This, however, will result in temperature overshoots. In order to minimise such overshoots, a third part which is proportional to the time derivative of the measured temperature is also added. This part controls the rate at which the temperature can be ramped. Thus, the total input power to the heater can be written as

$$W(t) = P\Delta(t) + I\int_{-\infty}^{t} \Delta(t)\, dt + D\frac{d}{dt}\Delta(t) \,. \tag{2.3}$$

The parameters **P, I,** and D are specific to a given oven and have to be tuned empirically. A detailed description of P I D controllers is given in Ref. [34].

2.4.3 Oven construction

The main body of the oven was made of a copper block with a slot for inserting the sample holder and inlet and outlet ports for the xrays. Two 40R Minco heating elements with kapton insulation were stuck to either sides of this block using a thin layers of heat resistant glue. Copper covering plates were used over the heating elements to improve the heat distribution. The sensor, a 100Ω platinum resistance thermometer (RTD), was inserted into a hole drilled into the copper block, very close to one of tne heating elements. The gaps were filled with heat-sink compound to ensure good thermal contact. The block was inserted into a teflon case with $\sim 0.5mm$ thick walls for heat insulation. The inlet and outlet ports were covered using $25\mu m$ thick mylar sheets. The sample holder was also made of copper and had holes for holding the sample capillary and for passing xrays. Another 100Ω RTD was fixed close to the sample to measure the sample temperature. Both the sample and the heater RTD's were calibrated with respect to a Minco standard RTD before assembling the oven. The magnetic field of about $0.6Tesla$ was generated by two ceramic magnets placed on either sides of the oven with a $1mm$ air gap to prevent direct thermal contact with the heater. A schematic diagram of the oven is shown in Fig. 2.23.

2.4.4 Temperature control

The sensor resistances were measured by the 4-probe method using a Keithley-2000 ($6\frac{1}{2}$ digits) digital multimeter equipped with a scanner card. The heater power was provided by an $HP6621A$ *d.c.* power supply with a total maximum output of 40V and 4A. Both the power supply and the multimeter were interfaced to a P.C. (086) using an HPIB interface card. A block diagram of the temperature control

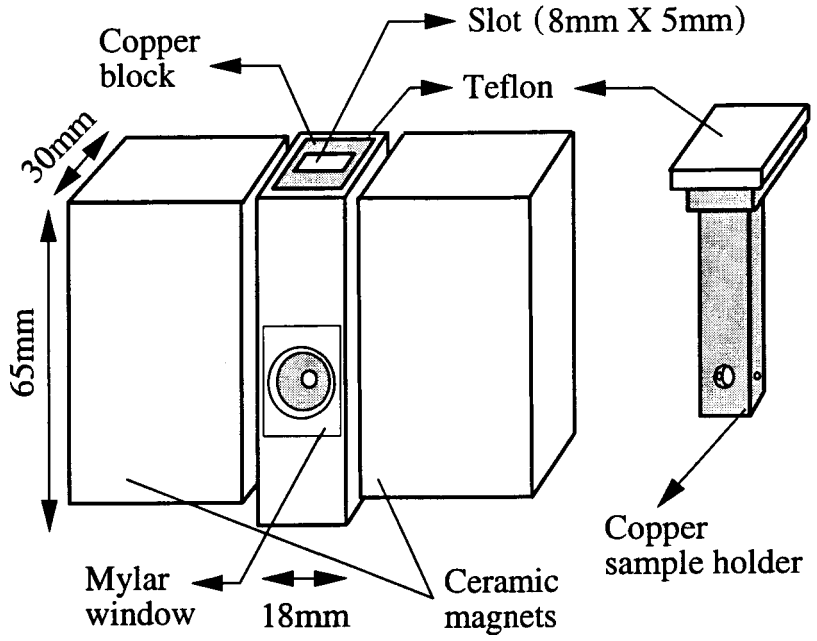

Figure **2.23:** A schematic drawing of the oven constructed for xray studies.

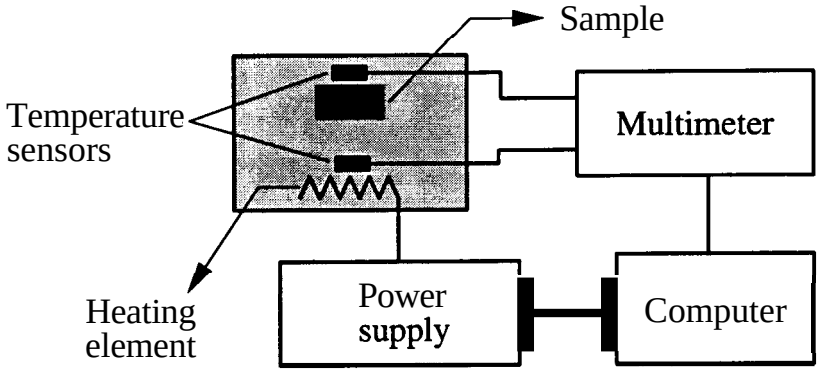

Figure 2.24: A schematic representation of the temperature control system.

system is shown in Fig. 2.24. The temperature was sampled every $2sec$, which was roughly equal to the response time of the oven. The computer code for controlling the instruments and for evaluating the PID terms was written in GW-Basic. The PID terms were calculated using a discretised version of Eq.2.3. The programme had the following main features:

- The temperature could be varied in specified steps and held at each step for a specified amount of time. This was essential for aligning the sample under the magnetic field.

- The PID parameters were tuned to give the best performance in a temperature range of about *60-80°C*.

- Different sets of parameters were used during heating and cooling. This is because the maximum cooling rate depends on the rate at which heat can be radiated off, whereas, the heating rate depends also on the amount of power that could be supplied.

- The coefficient of the proportional term was increased whenever the temperature had to be stepped by large values. In order to avoid overshoot, the parameters were changed back to the optimum value when the target temperature was approached and the value of the integral was replaced by one estimated for the heater temperature at that moment. To estimate the integral for various temperatures, the steady state power was measured at different temperatures and the data was fitted to a polynomial. This, of course, depends on the ambient temperature but was found to be a good starting value.

With these features the temperature of the sample could be controlled to an accuracy of $\pm 10mK$.